Published in final edited form as:

Cell Transplant. 2015 ; 24(9): 1813–1827. doi:10.3727/096368914X683025.

Intrathecal Transplantation of Autologous Adherent Bone Marrow Cells Induces Functional Neurological Recovery in a Canine Model of Spinal Cord Injury

Hala Gabr[*], **Wael Abo El-kheir**[†], **Haithem A. M. A. Farghali**[‡], **Zeinab M. K. Ismail**[§], **Maha B. Zickri**[§], **Zeinab M. El Maadawi**[§], **Nirmeen A. Kishk**[¶], and **Hatem E. Sabaawy**[*,#]

[*]Department of Hematology, Faculty of Medicine, Cairo University, Cairo, Egypt

[†]Department of Immunology, Military Medical Academy, Cairo, Egypt

[‡]Department of Veterinary Surgery, Anesthesiology and Radiology, Faculty of Veterinary Medicine, Cairo University, Cairo, Egypt

[§]Department of Histology, Faculty of Medicine, Cairo University, Cairo, Egypt

[¶]Department of Neurology, Faculty of Medicine, Cairo University, Cairo, Egypt

[#]Department of Medicine, Robert Wood Johnson Medical School, Rutgers University, and Rutgers Cancer Institute of New Jersey, New Brunswick, NJ, USA

Abstract

Spinal cord injury (SCI) results in demyelination of surviving axons, loss of oligodendrocytes, and impairment of motor and sensory functions. We have developed a clinical strategy of cell therapy for SCI through the use of autologous bone marrow cells for transplantation to augment remyelination and enhance neurological repair. In a preclinical large mammalian model of SCI, experimental dogs were subjected to a clipping contusion of the spinal cord. Two weeks after the injury, GFP-labeled autologous minimally manipulated adherent bone marrow cells (ABMCs) were transplanted intrathecally to investigate the safety and efficacy of autologous ABMC therapy. The effects of ABMC transplantation in dogs with SCI were determined using functional neurological scoring, and the integration of ABMCs into the injured cords was determined using histopathological and immunohistochemical investigations and electron microscopic analyses of sections from control and transplanted spinal cords. Our data demonstrate the presence of GFP-labeled cells in the injured spinal cord for up to 16 weeks after transplantation in the subacute SCI stage. GFP-labeled cells homed to the site of injury and were detected around white matter tracts and surviving axons. ABMC therapy in the canine SCI model enhanced remyelination and augmented neural regeneration, resulting in improved neurological functions. Therefore, autologous ABMC therapy appears to be a safe and promising therapy for spinal cord injuries.

Address Correspondence to Hatem E. Sabaawy, M.D., Ph.D., Regenerative and Molecular Medicine Program, Rutgers-Robert Wood Johnson Medical School, 195 Little Albany Street, New Brunswick, NJ 08901, USA. Tel: +1-732-235-8081; Fax: +1-732-235-8681; sabaawhe@rutgers.edu.

Keywords

Autologous adherent bone marrow-derived cell therapy; Spinal cord injury (SCI); Canine; Intrathecal; Remyelination

INTRODUCTION

Traumatic spinal cord injury (SCI) results in oligodendrocyte loss, demyelination of surviving axons, and severe functional impairment (28). Cell therapy is an attractive strategy to augment axonal sparing and remyelination and to overcome the physical and molecular barriers impeding repair (30). Cell types that may be used for autologous cell therapy of SCI include bone marrow (BM)- or adipose tissue-derived cells, olfactory ensheathing cells (OECs), Schwann cells, skin-derived precursor cells, and potentially induced pluripotent stem cells (iPSCs) or induced neuronal cells (14). Numerous preclinical studies, mostly utilizing rodent models of SCI, have demonstrated the efficacy of adult BM-derived cells in facilitating injury repair [reviewed in Tetzlaff et al. (42)]; however, the current consensus is that demonstrating efficacy in large mammalian models of SCI is necessary for clinical applications of cell therapy in SCI (23).

The BM contains multiple cell types that contribute differently to injury repair, and the fate and/or efficacy of these cells when delivered in vivo for cell therapy in SCI subjects are highly dependent on their harvest, isolation, propagation, and delivery procedures. Therefore, it is increasingly critical to distinguish the cell features and subtypes of BM-derived cells that are utilized for cell therapy investigations. The adult human BM in the iliac crest contains multiple heterogeneous stromal cells, including multipotent mesenchymal stromal cells (17) or mesenchymal stem cells (MSCs) (12) (the term “MSCs” is most frequently used to describe “culture-expanded” BM cells), adventitial reticular cells, vascular pericytes, BM fibroblasts, and bone-lining cells (19). All of the aforementioned BM stromal cell types contain cells that can self-renew, display a specific (and similar) set of surface phenotypes, and share the property of selective adherence to tissue culture plastic (8). The surface phenotypic markers that are present on BM stromal cells in vivo may be induced and/ or regulated by the BM microenvironment or be reflective of other cell functions in vivo that could potentially be lost upon plastic adherence and exposure to culture media for several weeks during the isolation and expansion of MSCs (18). Accordingly, we have developed a brief isolation procedure for BM stromal cells where we can exploit the adhesive property of these cells to isolate the “minimally manipulated” adherent BM cells (ABMCs), while they still maintain their in vivo phenotypic characteristics and (regenerative) features. We have previously isolated human ABMCs (12), and here we utilized a similar procedure to isolate canine ABMCs. We then examined the cell therapeutic abilities of these canine ABMCs for SCI repair through autologous transplantation, without culture expansion, in a preclinical canine model of SCI. Cell transplantations for SCI repair are frequently delivered at or near the site of injury or with systemic intravenous or intra-arterial infusions (40); however, cell delivery by intrathecal injections (24) is advantageous for clinical applications of autologous cell therapy.

ABMCs can contribute to injury repair by multiple mechanisms that are not completely understood. Direct differentiation of ABMCs into neural tissues has infrequently been achieved and remains contentious; however, evidence exists that ABMCs could be induced in vitro to differentiate into electrophysiologically responsive neuron-like cells (9,44,46), and BM mononuclear cells, containing ABMCs, were used to promote SCI repair in vivo in rodents, mammals, primates, and in pilot human studies (42). ABMCs also secrete cytokines, growth factors (38), and neurotrophic factors (2) that provide autocrine and paracrine support for damaged neural tissue. Moreover, ABMCs, after homing to sites of injury to deliver immunomodulatory and neuroprotective functions (29), enhance angiogenesis, reduce apoptosis and free radicals, and induce survival and regeneration of neurons (11).

We utilized autologous ABMCs for intrathecal transplantation to study the safety and neurological efficacy of this strategy in a canine model. SCI dogs treated with ABMCs achieved remarkable functional recovery, and no toxicities or side effects were observed. Moreover, we have recently reported on the safety and efficacy of a similar therapeutic strategy in a phase I/II trial encompassing 70 chronic SCI patients (13). Here we demonstrate the effects of intrathecal autologous ABMC transplantation in a canine model of SCI.

MATERIALS AND METHODS

Isolation and Culture of Canine ABMCs

Animal care and ABMC studies were carried out according to guidelines of the animal care committee of both Rutgers University and the Faculty of Medicine at Cairo University. Twenty-two adult male mixed-breed dogs (3 to 4 years old) were obtained from local vendors and housed at the vivarium of the Faculty of Veterinary Medicine at Cairo University. Canine ABMCs were isolated from the femurs of six adult dogs for in vitro studies, as we recently described for human ABMCs. Canine ABMCs were subjected to flow cytometry (FACSCalibur; BD Biosciences, San Jose, CA, USA) after staining with 100 µl of labeled antibodies (appropriately diluted to previously determined titration points) against the following cell surface markers: cluster of differentiation 13-phyco-erythrin (PE) cyanine 7 (cy7) (CD13-PC7), CD29-PC7, CD34-PE, CD44-fluorescein isothiocyanate (FITC), CD45-PC7, CD73-PE, CD90-PE, CD105-PE, CD166-PE, CD271-PE, and c-kit-PE (all from BD Biosciences). Dead cells were excluded by labeling with 1 µg/ml of 7-aminoac-tinomycin D (7-AAD; Invitrogen, Carlsbad, CA, USA). Mesenchymal induction into osteogenic, adipogenic, and chondrogenic lineages was performed as previously described (18,34). Green fluorescent protein (GFP) labeling and neural induction were performed as previously described (2,9) with modifications described below.

Neural Induction

ABMCs were isolated from the femurs of adult dogs. The low-density mononuclear cells were isolated using Ficoll-Plaque Plus (Amersham Biosciences, Pittsburgh, PA, USA). ABMCs were isolated by adherence on poly-L lysine-coated plates for 72 h, and nonadherent cells were removed by replacing the medium in three washing steps with

phosphate-buffered saline (PBS) including 0.5% selected prescreened fetal bovine serum (FBS; Hyclone, South Logan, UT, USA). ABMCs were maintained in Dulbecco's modified Eagle's medium (DMEM; Invitrogen)-low glucose supplemented with 10% FBS, 2 mg/ml L-glutamine (Gibco, Grand Island, NY, USA), and 0.3% penicillin streptomycin (Gibco) at 37°C and 5% CO_2 concentration. In vitro GFP labeling was done by adding pCMV-AcGFP plasmid mixed with lipofectamine at a 2:1 ratio to each plate and incubating at 37°C for 6 h before transplantation. Neural induction was performed as previously described (2,9) with some modifications. Neurosphere induction was done by culture in DMEM/Ham's F12 (1:1) supplemented with 2% (v/v) B27 medium (Invitrogen) and the growth factors epidermal growth factor (EGF; 20 ng/ml), basic fibroblast growth factor (bFGF; 20 ng/ml) (both from R&D Systems, Minneapolis, MN, USA), and heparin (5 μg/ml; Sigma-Aldrich, St. Louis, MO, USA). Three-dimensional semi-floating neurosphere-like collections appeared after 4–7 days. Neuronal induction was done by using single cells that were lifted by incubation with accutase (Invitrogen) at 37°C for 3–4 min and plated at a density of 2,000 cells/cm^2 in serum-free DMEM/F12, with 2% (v/v) FBS, 2% (v/v) B27 medium (Invitrogen), bFGF (20 ng/ml), and all-*trans*-retinoic acid (RA; 20 μM; Sigma-Aldrich). Cells were kept under these conditions for 12 days and were then fixed, stained with primary and secondary antibodies, and analyzed by immunofluorescence microscopy.

Immunostaining

Cells were fixed in 4% paraformaldehyde and stored under PBS at 4°C until stained. To assess the histopathological changes, all dogs were euthanized at 16 weeks after the cell therapy. The histological analysis was blinded until completion of the study. Dogs were perfused with 0.14 M Sorensen's phosphate buffer and 4% paraformaldehyde (Sigma-Aldrich), pH 7.4, and spinal cords from T10 to L5 were fixed in 10% buffered neutral formalin (Sigma-Aldrich) and immersed in a decalcifying solution. Sections were either embedded in paraffin, and 4-μm-thick axial sections were cut for histological and IHC analyses, or prepared for plastic embedding by postfixing with 1% osmium tetroxide (Electron Microscopy Sciences, Hatfield, PA, USA), dehydrating in graded ethanol solutions, embedding in Epox (Electron Microscopy Sciences), and 90-μm-thick axial sections were cut for electron microscopy analysis. Paraffin sections were stained with hematoxylin and eosin (H&E), Luxol fast blue (both from Sigma-Aldrich) to identify myelin or used for fluorescence analyses. Myelinated areas and volumes of the cavities from the epicenter of the damaged spinal cord were calculated from images of the transverse sections using AxioVision image analysis software (Carl Zeiss Microimaging GmbH, Jena, Germany). The section was identified with the largest area of cavitation, and this area was measured for each dog and expressed as mean ± SD from control and cell therapy-treated dogs. For immunofluorescence, the deparaffinized sections were processed through antigen retrieve for 2 min and then stained with specific antibodies appropriate for canine cross-reactivity. Primary antibodies were monoclonal anti-GFP (1:100; Clontech Laboratories, Inc., Mountain View, CA, USA), monoclonal anti-microtubule-associated protein 2 (MAP2) (1:500; Sigma-Aldrich), polyclonal anti-glial fibrillary acidic protein (GFAP) (1:500; Dako, Carpinteria, CA, USA), monoclonal anti-type III β-tubulin epitope J1 (TuJ1; 1:200; Chemicon, Billerica, MA, USA), polyclonal anti-platelet-derived growth factor receptor-α (PDGFRα; 1:80; Chemicon), monoclonal anti-glutamic acid decarboxylase, 65 kDa isoform

(GAD65; 1:500; Abcam, Cambridge, MA, USA), polyclonal anti-nestin (1:100; LifeSpan Biosciences, Inc., Seattle, WA, USA), monoclonal anti-acetylcholinestrase (AE-1; 1:50; Millipore, Billerica, MA, USA), monoclonal anti-70 kDa neurofilament (NF70; 1:50; Millipore), monoclonal antineuron cell surface antigen clone A2B5-105 (A2B5) (1:100; Millipore), and monoclonal anti-metabotropic glutamate receptor 1 (GRM1; 1:100; BD). Peroxidase ABC kit and $CoCl_2$-enhanced diaminobenzidine (DAB) (Fisher Scientific, Pittsburgh, PA, USA) were used as chromagen for myelin basic protein (MBP) staining. For fluorescent microscopy, secondary antibodies labeled with Alexa Fluor 488, 535, and 610 dyes (Invitrogen) were employed. Nuclear counterstaining using 1 μg/ml of 4′,6-diamidino-2-phenylindole (DAPI; Invitrogen) in 400 μl was performed. A bacterial artificial chromosome (BAC) containing canine chromosome 35 (a kind gift from Ming Yao, Rutgers University) was used as a probe for fluorescent in situ hybridization (FISH) to detect cell fusion. The targeted area chosen for calculating GFP, nestin, PDGFR, TuJ1, and NF70 counts used 100 squares with a surface area of 0.01 mm^2 each. Values are presented as mean ± SD. Histologists who were blinded to therapy performed histological examinations.

Canine Model of Spinal Cord Injury

Sixteen healthy adult mixed-breed male dogs that weighed 3.77 ± 0.59 kg were used for the experimental SCI study. All aspects of animal care and treatments were approved by the animal care committee of Cairo University. Anesthetized dogs (with sodium pentobarbital, 40 mg/kg, University Pharmacy) were placed in ventral recumbency on the operating bed and received a spinal cord injury at the L4 level performed by the same veterinary neurosurgeon on all 16 dogs. Briefly, after L4 laminectomy, the dura was opened, and the spinal cord was subjected to a guided fixed length clipping contusion to ensure reproducibility of the lesion. Postoperative care included that the dogs were kept warm and given manual bladder evacuation twice per day and prophylactic antibiotics. The dogs had no difficulty in feeding. The dogs were randomly assigned, without bias, to four groups according to treatment after SCI (n = 4/group), with group A serving as controls receiving no cell treatment. Group B, C, and D dogs received 2×10^6 GFP-labeled ABMCs/kg by lumbar puncture. Group B animals received unmanipulated ABMCs. To investigate whether in vitro neural induction of ABMCs would augment their in vivo repair potential, groups C and D animals received ABMCs isolated at 72 h that were induced in neural media for either the last 24 h (group C) or for a full 72 h (group D). Transplantation of canine ABMCs was performed 2 weeks after the SCI. The dogs were anesthetized using the same methods described above. Fifty milliliters of BM were aspirated from each side of the iliac crest, and ABMCs were isolated by adherence for 72 h as described above. In the three groups (B–D) receiving unmanipulated ABMCs or ABMCs induced for neural differentiation for 24 or 72 h, respectively, cells suspended in 150 μl of saline solution were transplanted by an intrathecal injection into the CSF by lumbar puncture using a 22-gauge spinal needle. Behavioral assessments of hindlimb functional recovery were done by video recording. Each dog was videotaped from the sides and back for a minimum of 10 walking steps. Dogs with limited weight bearing were supported in place by holding the base of their tail. Using a 15-point scoring system (31), the gait of each dog was independently scored from the videotapes by two investigators blinded to treatment type, and the mean scores at baseline, 1 day after SCI, and at 2, 4, 8, 12, and 16 weeks after SCI were recorded.

Data Analysis

For quantitative analysis of transplanted GFP cells in the spinal cord, 15 cross sections were cut from each dog's spinal cord at 4 μm thickness, 150 μm apart. All cells in each section with an average of 6 μM in diameter were counted. Three sections of spinal cord per antibody were examined for double-positive cells, and four regions per section were counted. For the functional testing, differences in locomotor scores between transplanted dogs and controls were analyzed by blinded examiners at each time point. All data were expressed as mean ± SD. In vitro data and quantitative variables for outcome among transplanted and control dogs were compared using Student's *t*-test when applicable. Group outcome statistics among subgroups of transplanted and control dogs were compared using two-sample Wilcoxon rank-sum (Mann–Whitney) test or Fisher's exact test among all groups using Microsoft Excel (Redmond, WA, USA), Sigmaplot (Systat Software, San Jose, CA, USA), or Stata software (Stata, College Station, TX, USA) unless otherwise specified. Statistical significance was determined at a value of $p < 0.05$.

RESULTS

In Vitro Differentiation of ABMCs

Six normal canine BM samples were subjected to adherence for 72 h on poly-L-lysine under an approved protocol. Canine ABMCs expressed CD29, CD44, CD73, CD90, CD105, CD117 (C-Kit), CD166, and CD271, but had very low (<0.01%) to no detectable expression of CD45, CD34, and CD13 (Fig. 1). Thus, ABMCs share some phenotypic features with canine MSCs that were positive for CD90 and lacked expression of CD34 and CD45 and could be neurally induced (20). Canine ABMCs had a flat oblong morphology (Fig. 2A) with few fibroblast-like cells that frequently predominate the traditional culture-expanded MSCs. Canine ABMCs were transfected with GFP-expressing plasmid at ~90% efficiency (Fig. 2B). The expression of GFP in these cells had no detectable effect on their morphology (Fig. 2B) nor on their response to either mesenchymal or neural induction (not shown). Culture of these cells in neural induction medium, similar to human cells (5), resulted in the formation of atypical neurospheres (Fig. 2C). These ABMCs could be potentially induced to adipocytes, osteocytes, and chondrocytes (Fig. 2D–F). Morphological changes with increased expression of the neuronal dendrite-specific MAP2 in cells with neural-like morphology were evident following neural induction (Fig. 2G–L).

Neurological Functional Recovery in ABMC-Treated Canine SCI Model

Clipping contusions to the dog spinal cord performed on 16 dogs resulted in sensory loss and bilateral hindlimb paralysis with no residual motor or sensory functions in all injured dogs. One week after injury, animals regained some ability for weight support at least on one side due to spontaneous recovery. These effects reached plateau after 2 weeks, and untreated dogs remained with limited hindlimb weight-bearing abilities for the duration of the studies. Locomotor performance and functional recovery of hindlimbs were evaluated every 4 weeks for 16 weeks after transplantation using a 15-point videotaping scoring system developed for canine SCI (31) (Fig. 3). Motor function of the hindlimbs was intact before SCI, and all animals scored 14–15 points (Fig. 3A). After injury, dogs were paraplegic with no deep pain sensation, and hindlimb scores neared zero. No significant differences were measured

statistically between the three groups of dogs B, C, and D, receiving unmanipulated or induced ABMCs (Table 1). Dogs receiving autologous ABMC transplant (from groups B, C, and D; $n = 12$) reached near maximum recovery at 8 weeks posttransplant (Fig. 3A and Table 1), with a significant recovery ($p < 0.001$ when compared to controls) of their motor function. These effects were associated with enhanced spontaneous hindlimb movements (Fig. 3B) 1 week after therapy, suggesting early neuroprotective effects of ABMCs. At 16 weeks posttreatment, dogs were euthanized, and spinal cords were fixed for histology and immunostaining. Sections of injured spinal cord from control dogs showed severe vacuole formation, in contrast to reduced residual cavitation in group B ABMC-treated sections (Figs. 3C–E and 4). Immunostaining with anti-MBP antibody was increased in ABMC-treated dogs compared to controls and reached up to 85% of MBP levels in intact cords (Fig. 3F–I), suggesting potential remyelination.

Localization of ABMCs at the Spinal Cord Injury Site

We performed multicolor immunohistochemistry (with sections from control and group B dogs) using GFP as a marker for transplanted autologous minimally manipulated ABMCs in association with spinal cord resident neural cell markers (Fig. 5). Once again, less cavitation in the gray and white matter was noticed in ABMC-treated sections (Fig. 5A, B), and GFP^+ cells were detected within the SCI lesion boundaries (Fig. 5C–H). GFP^+ cells were widely distributed from the epicenter and were found in the gray and white matter of the injured cord and distributed at the lesion boundary zone, around the central canal, and in the contralateral gray matter (Fig. 5F). On average, 29 ± 5% of GFP^+ cells in the white (Fig. 5C–E and G–H) and gray matter (Fig. 5I–K) were also positive for NF70, a specific marker for mature neurons. The dorsal funiculus of the spinal cord consists largely of myelinated axons. GFP staining was also observed in the dorsal funiculus with several cells expressing NF70 (Fig. 5L–N). ABMC-derived cells positive for both GFP and either the neural progenitor marker nestin in a high-density synaptic apposition (Fig. 5O), the oligodendrocyte precursor marker PDGFR in a lower-density synaptic apposition (Fig. 5P), or the astrocyte precursor marker GFAP in nerve bundles (Fig. 5Q) were found. Moreover, ABMC-derived cells positive for both GFP and PDGFR were seen near microvessels surrounding the central canal (Fig. 6A). No GFP^+ cells were detected in controls (Fig. 6C–F) as expected, while GFP^+ cells expressing NF70 were found within cross sections of the ventral roots (Fig. 6G–J) of ABMC-treated dogs.

The distribution of GFP^+ cells reflected a prototype favoring regeneration. We detected a number of GFP^+ cells expressing NF70 within cross sections of the ventral funiculus area (area 3 in Fig. 5B) that is known to contain anterior corticospinal tracts. The localization of GFP^+ ABMC-derived cells near the anterior corticospinal tracts, controlling voluntary movements and traditionally valued as least capable of regeneration (4), suggests more robust regeneration with ABMCs. We observed infrequent GFP^+ cells that colocalized with A2B5, a ganglioside antigen present in common glial precursors O-2A (data not shown) with neural stem cell features. Furthermore, the predominance of double-labeled profiles of GFP^+ cells expressing neural progenitor markers was seen in both gray and white matter. GFP^+ cells expressed markers of the resident neural precursor tissues involved in inducing terminal neural cell fate, as suggested by detection of GFP^+ cells, though in limited

numbers, that colocalized with excitatory, inhibitory, and cholinergic neurotransmitter markers. Cells dually labeled with GFP and either excitatory GRM1, inhibitory GAD as a marker for GABAergic signals, or cholinergic AE-1 signals were detected at low frequencies (<1%) (Fig. 7).

Molecular and Electron Microscopic Features of ABMC-Induced Remyelination

First, to exclude the possible occurrence of fusion events as a mechanism for injury repair and regeneration, we analyzed sections of canine spinal cords that were subjected to grafting experiments. DAPI nuclear-stained GFP-expressing cells were examined using a canine chromosome 35 FISH probe. All examined cells (n = 500) were diploid (not shown), suggesting that fusion events were not present. Moreover, electron micrographs in sections from control animals demonstrated demyelinated axons, extensive vacuolation, and glial scarring in an extracellular environment free of astrogliosis. In contrast, electron micrographs of similar sections from ABMC-treated animals demonstrated a larger number of myelinated axons (compare Fig. 8D vs. A). Analysis of these electron micrographs of sections from autologous ABMC-transplanted dogs (Fig. 8D) demonstrated that remyelinated axons appear predominantly associated with peripheral-like myelin-forming cells. Oligodendrocyte-myelinated axons with central myelination and characteristic thin myelin sheaths were observed in the smaller axons (Fig. 8E, F) in only one third of the total remyelinated axons. Remyelinated axons were associated with astrocytes characterized by multilobular nucleoli and large intermediate filament-rich processes that extended to multiple remyelinated axons (Fig. 8G, H) and occasionally to thickly remyelinated axons (Fig. 8I). Collectively, these data suggest that ABMCs drive injury repair, remyelination, and potential neural regeneration within the injured spinal cord microenvironment.

DISCUSSION

Our studies demonstrate that intrathecal transplantation of autologous canine ABMCs contributes considerably to the inadequate axonal regeneration in mammalian SCI (30). Stem cell therapy is beneficial for SCI repair (39), and the multiple beneficial mechanisms by which ABMC therapy repairs injuries suggest that ABMC transplantation achieves an initial preclinical efficacy (23) in a large mammalian SCI model. These data are in accordance with the beneficial effects seen with ABMC transplantation in human SCI patients based on the initial outcome data of our phase I/II clinical trial (13). Intrathecal transplantation of autologous ABMCs in the canine SCI model was associated with remyelination and functional improvement. These repair features that are translated from pre-clinical models to SCI patients are unique to BM-derived cells (4,8,43), considering that transplantation of OECs showed functional benefits in rats (25) and pet dogs with SCI (15) but had modest outcome in SCI patients (27). Moreover, neural stem cells (NSCs) were recently shown to exert remarkable axonal growth and induce functional repair in the rat SCI model (26); however, transplanted NSCs that are rather derived from embryos have been linked to brain tumor development in an ataxia telangiectasia patient (1). Therefore, the long-term safety profile of allogeneic and fetal-derived neural progenitor and potentially iPSC-derived cell transplantation requires added scrutiny before wide clinical applications. Indeed, autologous cell therapy for SCI remains to date a more safe and feasible strategy.

BM cells with limited culture expansion have been used in pilot studies and human clinical trials to improve neurological functions when delivered near the injury site via intra-arterial (40) and intrathecal injections (13,22) in chronic SCI patients. Importantly, all human trials demonstrate the superior safety profile of BM-derived cells (8,42).

Delayed transplantation in subacute SCI perhaps acts in a more permissive, “less inflammatory” environment supporting graft survival. Additionally, intrathecal delivery of ample BM cells is likely to be more effective when compared to systemic delivery and homing of a fraction of the injected BM cells (21,40). At the functional level, ABMCs act to repair SCI by multiple nonmutually exclusive mechanisms. Neural regeneration likely plays a modest role, either directly (33) or through recruitment of either brain neural crest stem cells that mature into Schwann cells or spinal cord ependymal stem cells. We found the largest number of GFP^+ ABMC-derived cells around the central canal, where ependymal cells reside (3,36), suggesting that ependymal cells might be implicated in the repair process. Moreover, analyses of electron micrographs from transplanted dogs suggest that axons were remyelinated by Schwann cells that have a guidance role in axonal regeneration and myelination. In particular, osteopontin and clusterin derived from Schwann cells were recently shown to play a significant role in regeneration of peripheral motor and sensory axons (47) and may play similar roles when secreted from ABMCs, ABMC-derived Schwann or other cell types, and/or cells instructed by ABMC-signaling mediators during SCI regeneration. ABMCs also produce neurotrophic factors and anti-inflammatory mediators (29) that support spinal cord tissue by creating new neuronal pathways in fibrous scar tissues (10) or by expanding sprouting or generating short regenerated neural fibers (28). Another mechanism was revealed when BM-derived cells reversed proinflammatory M1 macrophages into M2 anti-inflammatory macrophages with reduced matrix metalloproteinase-9 release, therefore effectively preventing the induction of axonal dieback (6). In addition to these effects on macrophages, BM-derived cells also promoted sensory neurite outgrowth, induced sprouting, and increased neurite intrinsic growth capacity, further enabling axons to overcome the negative effects of inhibitory proteoglycans and M1 macrophages (6). Furthermore, it has been recently reported that the antihelmintic drug fenbendazole surprisingly reversed the effects of contusive SCI in mice (48). Immune response and autoantibodies produced after SCI contribute to axon damage, and eliminating these antibodies through the anti-inflammatory mediators secreted by ABMCs might be beneficial for regeneration. Additionally, ABMCs, or their secreted exosome products, may control the expression of microRNAs that are critical for SCI repair (49) or contain cells that provide guidance for connection to distal and proximal ends of the spinal cord and therefore facilitate regeneration (16).

ABMCs injected intrathecally were minimally manipulated BM cells and were not the culture-expanded MSCs. Furthermore, neural induction of ABMCs in vitro prior to transplantation had no benefit. Prolonged culture may alter the biological, phenotypic, immunomodulatory, and differentiation capacities of these cells (35). The identities of the BM cells that gave rise to myelin-forming cells that may have induced neural regeneration remain elusive. Since transplantation of $CD34^+$ cells in similar conditions did not result in myelination (37), while transplantation of $CD34^-$ BMCs resulted in functional improvement (7); therefore, $CD34^+$ cells are not likely candidate repair cells. Potential candidates include

nonhematopoietic cells that have multipotent activity and share surface marker phenotypes, such as multipotent mesenchymal stromal cells, adventitial reticular cells, vascular pericytes, bone-lining cells (19), and fibroblasts or perhaps a number of these cell types each contributing uniquely to a cooperative repair process. In light of the induced pluripotency of adult fibroblasts (41) or the potential conversion of neonatal fibroblasts to functional neurons (32,45), we cannot exclude the possibility that BM-derived fibroblasts participate in injury repair in response to clues in the spinal cord microenvironment. Additionally, the vast majority of cell bodies and nuclei present within the lesion zone of our repaired spinal cords were associated with myelin-forming cells, suggesting that remyelinating cells were the predominant cell type to differentiate. Likewise, it is possible that ABMCs or their derivative cells are reprogrammed in vivo to adapt to or exhibit a remyelinating fate in response to clues in the SCI microenvironment. Further studies interrogating each of these potential mechanisms of repair will shed light on the role(s) of ABMCs in mediating SCI repair and allow for defining targets for an added enhancement of these repair features to achieve a more significant neural regeneration. In conclusion, autologous grafting of ABMCs, harvested from the patient's own BM, without ethical or immunological concerns, might be an effective therapeutic strategy to provide neurological functional improvement. This strategy may be implemented for cell therapy of pet dogs suffering from SCI and is translated to enhance the quality of life of human SCI patients.

Acknowledgments

We thank Drs. Joseph Bertino (The Stem Cell Institute of New Jersey), Robert DiPaola (The Cancer Institute of New Jersey), Pranela Rameshwar (Rutgers-New Jersey Medical School), George Heinrich (Rutgers-New Jersey Medical School), and Mervat El Ansary (Cairo University School of Medicine) for helpful discussions. We thank Dr. S. R. Pine (The Cancer Institute of New Jersey) for assistance with flow cytometry, and Lei Cong for assistance with histological and immunohistochemical staining. We also appreciate the excellent work of all personnel at the Central Hematology Laboratory, Department of Clinical Pathology, Faculty of Medicine, Cairo University. This work was generously supported by Rutgers Cancer Institute of New Jersey, New Jersey Health Foundation, Cairo University, and the Egyptian Academy for Scientific Research and Technology. H.E.S. is a founder and stockholder, and H.G. and W.A.E. are collaborators of Celvive, Inc., a company that has licensed the cell therapy technology from Rutgers University. We thank the New Jersey Health Foundation for funding of the follow-up studies through Celvive, Inc. All of the other authors declare no conflicts of interest.

References

1. Amariglio N, Hirshberg A, Scheithauer BW, Cohen Y, Loewenthal R, Trakhtenbrot L, Paz N, Koren-Michowitz M, Waldman D, Leider-Trejo L, Toren A, Constantini S, Rechavi G. Donor-derived brain tumor following neural stem cell transplantation in an ataxia telangiectasia patient. PLoS Med. 2009; 6(2):e1000029. [PubMed: 19226183]
2. Arnhold S, Klein H, Klinz FJ, Absenger Y, Schmidt A, Schinkothe T, Brixius K, Kozlowski J, Desai B, Bloch W, Addicks K. Human bone marrow stroma cells display certain neural characteristics and integrate in the subventricular compartment after injection into the liquor system. Eur. J Cell Biol. 2006; 85(6):551–565.
3. Barnabe-Heider F, Goritz C, Sabelstrom H, Takebayashi H, Pfrieger FW, Meletis K, Frisen J. Origin of new glial cells in intact and injured adult spinal cord. Cell Stem Cell. 2010; 7(4):470–482. [PubMed: 20887953]
4. Blesch A, Tuszynski MH. Spinal cord injury: Plasticity, regeneration and the challenge of translational drug development. Trends Neurosci. 2009; 32(1):41–47. [PubMed: 18977039]
5. Bossolasco P, Cova L, Calzarossa C, Rimoldi SG, Borsotti C, Deliliers GL, Silani V, Soligo D, Polli E. Neuro-glial differentiation of human bone marrow stem cells in vitro. Exp Neurol. 2005; 193(2): 312–325. [PubMed: 15869934]

6. Busch SA, Hamilton JA, Horn KP, Cuascut FX, Cutrone R, Lehman N, Deans RJ, Ting AE, Mays RW, Silver J. Multipotent adult progenitor cells prevent macrophage-mediated axonal dieback and promote regrowth after spinal cord injury. J Neurosci. 2011; 31(3):944–953. [PubMed: 21248119]
7. Carvalho KA, Cunha RC, Vialle EN, Osiecki R, Moreira GH, Simeoni RB, Francisco JC, Guarita-Souza LC, Oliveira L, Zocche L, Olandoski M. Functional outcome of bone marrow stem cells (CD45(+)/CD34(−)) after cell therapy in acute spinal cord injury: In exercise training and in sedentary rats. Transplant Proc. 2008; 40(3):847–849. [PubMed: 18455034]
8. Charbord P. Bone marrow mesenchymal stem cells: Historical overview and concepts. Hum Gene Ther. 2010; 21(9):1045–1056. [PubMed: 20565251]
9. Cho KJ, Trzaska KA, Greco SJ, McArdle J, Wang FS, Ye JH, Rameshwar P. Neurons derived from human mesenchymal stem cells show synaptic transmission and can be induced to produce the neurotransmitter substance P by interleukin-1 alpha. Stem Cells. 2005; 23(3):383–391. [PubMed: 15749933]
10. Cregg JM, Depaul MA, Filous AR, Lang BT, Tran A, Silver J. Functional regeneration beyond the glial scar. Exp Neurol. 2014; 253C:197–207.
11. Crigler L, Robey RC, Asawachaicharn A, Gaupp D, Phinney DG. Human mesenchymal stem cell subpopulations express a variety of neuro-regulatory molecules and promote neuronal cell survival and neuritogenesis. Exp Neurol. 2006; 198(1):54–64. [PubMed: 16336965]
12. Ding DC, Shyu WC, Lin SZ. Mesenchymal stem cells. Cell Transplant. 2011; 20(1):5–14. [PubMed: 21396235]
13. El-Kheir WA, Gabr H, Awad MR, Ghannam O, Barakat Y, Farghali HA, Maadawi ZM, Ewes I, Sabaawy HE. Autologous bone marrow-derived cell therapy combined with physical therapy induces functional improvement in chronic spinal cord injury patients. Cell Transplant. 2014; 23(6):729–745. [PubMed: 23452836]
14. Fehlings MG, Vawda R. Cellular treatments for spinal cord injury: The time is right for clinical trials. Neurotherapeutics. 2011; 8(4):704–720. [PubMed: 22002087]
15. Granger N, Blamires H, Franklin RJ, Jeffery ND. Autologous olfactory mucosal cell transplants in clinical spinal cord injury: A randomized double-blinded trial in a canine translational model. Brain. 2012; 135(Pt 11):3227–3237. [PubMed: 23169917]
16. Hofstetter CP, Schwarz EJ, Hess D, Widenfalk J, El Manira A, Prockop DJ, Olson L. Marrow stromal cells form guiding strands in the injured spinal cord and promote recovery. Proc Natl Acad Sci USA. 2002; 99(4):2199–2204. [PubMed: 11854516]
17. Horwitz EM, Le Blanc K, Dominici M, Mueller I, Slaper-Cortenbach I, Marini FC, Deans RJ, Krause DS, Keating A. Clarification of the nomenclature for MSC: The International Society for Cellular Therapy position statement. Cytotherapy. 2005; 7(5):393–395. [PubMed: 16236628]
18. in ‘t Anker PS, Noort WA, Scherjon SA, Kleijburgvan der Keur C, Kruisselbrink AB, van Bezooijen RL, Beekhuizen W, Willemze R, Kanhai HH, Fibbe WE. Mesenchymal stem cells in human second-trimester bone marrow, liver, lung, and spleen exhibit a similar immunophenotype but a heterogeneous multilineage differentiation potential. Haematologica. 2003; 88(8):845–852. [PubMed: 12935972]
19. Jones E, McGonagle D. Human bone marrow mesenchymal stem cells in vivo. Rheumatology. 2008; 47(2):126–131. [PubMed: 17986482]
20. Kamishina H, Deng J, Oji T, Cheeseman JA, Clemmons RM. Expression of neural markers on bone marrow-derived canine mesenchymal stem cells. Am J Vet Res. 2006; 67(11):1921–1928. [PubMed: 17078756]
21. Karp JM, Leng Teo GS. Mesenchymal stem cell homing: The devil is in the details. Cell Stem Cell. 2009; 4(3):206–216. [PubMed: 19265660]
22. Kishk NA, Gabr H, Hamdy S, Afifi L, Abokresha N, Mahmoud H, Wafaie A, Bilal D. Case control series of intrathecal autologous bone marrow mesenchymal stem cell therapy for chronic spinal cord injury. Neurorehabil Neural Repair. 2010; 24(8):702–708. [PubMed: 20660620]
23. Kwon BK, Soril LJ, Bacon M, Beattie MS, Blesch A, Bresnahan JC, Bunge MB, Dunlop SA, Fehlings MG, Ferguson AR, Hill CE, Karimi-Abdolrezaee S, Lu P, McDonald JW, Müller HW, Oudega M, Rosenzweig ES, Reier PJ, Silver J, Sykova E, Xu XM, Guest JD, Tetzlaff W.

Demonstrating efficacy in preclinical studies of cellular therapies for spinal cord injury – How much is enough? Exp Neurol. 2013; 248:30–44. [PubMed: 23727091]

24. Lee J, Kuroda S, Shichinohe H, Ikeda J, Seki T, Hida K, Tada M, Sawada K, Iwasaki Y. Migration and differentiation of nuclear fluorescence-labeled bone marrow stromal cells after transplantation into cerebral infarct and spinal cord injury in mice. Neuropathology. 2003; 23(3):169–180. [PubMed: 14570283]
25. Lopez-Vales R, Fores J, Navarro X, Verdu E. Chronic transplantation of olfactory ensheathing cells promotes partial recovery after complete spinal cord transection in the rat. Glia. 2007; 55(3):303–311. [PubMed: 17096411]
26. Lu P, Wang Y, Graham L, McHale K, Gao M, Wu D, Brock J, Blesch A, Rosenzweig ES, Havton LA, Brock J, Blesch A, Rosenzweig ES, Havton LA. Long-distance growth and connectivity of neural stem cells after severe spinal cord injury. Cell. 2012; 150(6):1264–1273. [PubMed: 22980985]
27. Mackay-Sim A, Feron F, Cochrane J, Bassingthwaighte L, Bayliss C, Davies W, Fronek P, Gray C, Kerr G, Licina P, Nowitzke A, Perry C, Silburn PA, Urquhart S, Geraghty T. Autologous olfactory ensheathing cell transplantation in human paraplegia: A 3-year clinical trial. Brain. 2008; 131(Pt 9):2376–2386. [PubMed: 18689435]
28. McDonald JW, Sadowsky C. Spinal-cord injury. Lancet. 2002; 359(9304):417–425. [PubMed: 11844532]
29. Nauta AJ, Fibbe WE. Immunomodulatory properties of mesenchymal stromal cells. Blood. 2007; 110(10):3499–3506. [PubMed: 17664353]
30. Nishio T. Axonal regeneration and neural network reconstruction in mammalian CNS. J Neurol. 2009; 256(Suppl 3):306–309. [PubMed: 19711121]
31. Olby NJ, De Risio L, Munana KR, Wosar MA, Skeen TM, Sharp NJ, Keene BW. Development of a functional scoring system in dogs with acute spinal cord injuries. Am J Vet Res. 2001; 62(10): 1624–1628. [PubMed: 11592330]
32. Pang ZP, Yang N, Vierbuchen T, Ostermeier A, Fuentes DR, Yang TQ, Citri A, Sebastiano V, Marro S, Sudhof TC, Wernig M. Induction of human neuronal cells by defined transcription factors. Nature. 2011; 476(7359):220–223. [PubMed: 21617644]
33. Patel N, Klassert TE, Greco SJ, Patel SA, Munoz JL, Reddy BY, Bryan M, Campbell N, Kokorina N, Sabaawy HE, Rameshwar P. Developmental regulation of TAC1 in peptidergic-induced human mesenchymal stem cells: Implication for spinal cord injury in zebrafish. Stem Cells Dev. 2012; 21(2):308–320. [PubMed: 21671725]
34. Pittenger MF, Mackay AM, Beck SC, Jaiswal RK, Douglas R, Mosca JD, Moorman MA, Simonetti DW, Craig S, Marshak DR. Multilineage potential of adult human mesenchymal stem cells. Science. 1999; 284(5411):143–147. [PubMed: 10102814]
35. Prockop DJ. Repair of tissues by adult stem/progenitor cells (MSCs): Controversies, myths, and changing paradigms. Mol Ther. 2009; 17(6):939–946. [PubMed: 19337235]
36. Sabelstrom H, Stenudd M, Reu P, Dias DO, Elfineh M, Zdunek S, Damberg P, Goritz C, Frisen J. Resident neural stem cells restrict tissue damage and neuronal loss after spinal cord injury in mice. Science. 2014; 342(6158):637–640.
37. Sasaki M, Honmou O, Akiyama Y, Uede T, Hashi K, Kocsis JD. Transplantation of an acutely isolated bone marrow fraction repairs demyelinated adult rat spinal cord axons. Glia. 2001; 35(1): 26–34. [PubMed: 11424189]
38. Schinkothe T, Bloch W, Schmidt A. In vitro secreting profile of human mesenchymal stem cells. Stem Cells Dev. 2008; 17(1):199–206. [PubMed: 18208373]
39. Snyder EY, Teng YD. Stem cells and spinal cord repair. N Engl J Med. 2012; 366(20):1940–1942. [PubMed: 22591301]
40. Sykova E, Homola A, Mazanec R, Lachmann H, Konradova SL, Kobylka P, Padr R, Neuwirth J, Komrska V, Vavra V, Stulík J, Bojar M. Autologous bone marrow transplantation in patients with subacute and chronic spinal cord injury. Cell Transplant. 2006; 15(8–9):675–687. [PubMed: 17269439]
41. Takahashi K, Yamanaka S. Induction of pluripotent stem cells from mouse embryonic and adult fibroblast cultures by defined factors. Cell. 2006; 126(4):663–676. [PubMed: 16904174]

42. Tetzlaff W, Okon EB, Karimi-Abdolrezaee S, Hill CE, Sparling JS, Plemel JR, Plunet WT, Tsai EC, Baptiste D, Smithson LJ, Kawaja MD, Fehlings MG, Kwon BK. A systematic review of cellular transplantation therapies for spinal cord injury. J Neurotrauma. 2011; 28(8):1611–1682. [PubMed: 20146557]

43. Thuret S, Moon LD, Gage FH. Therapeutic interventions after spinal cord injury. Nat Rev Neurosci. 2006; 7(8):628–643. [PubMed: 16858391]

44. Tropel P, Platet N, Platel JC, Noel D, Albrieux M, Benabid AL, Berger F. Functional neuronal differentiation of bone marrow-derived mesenchymal stem cells. Stem Cells. 2006; 24(12):2868–2876. [PubMed: 16902198]

45. Vierbuchen T, Ostermeier A, Pang ZP, Kokubu Y, Sudhof TC, Wernig M. Direct conversion of fibro-blasts to functional neurons by defined factors. Nature. 2010; 463(7284):1035–1041. [PubMed: 20107439]

46. Wislet-Gendebien S, Hans G, Leprince P, Rigo JM, Moonen G, Rogister B. Plasticity of cultured mesenchymal stem cells: Switch from nestin-positive to excitable neuron-like phenotype. Stem Cells. 2005; 23(3):392–402. [PubMed: 15749934]

47. Wright MC, Mi R, Connor E, Reed N, Vyas A, Alspalter M, Coppola G, Geschwind DH, Brushart TM, Hoke A. Novel roles for osteopontin and clusterin in peripheral motor and sensory axon regeneration. J Neurosci. 2014; 34(5):1689–1700. [PubMed: 24478351]

48. Yu CG, Singh R, Crowdus C, Raza K, Kincer J, Geddes JW. Fenbendazole improves pathological and functional recovery following traumatic spinal cord injury. Neuroscience. 2014; 256:163–169. [PubMed: 24183965]

49. Yu YM, Gibbs KM, Davila J, Campbell N, Sung S, Todorova TI, Otsuka S, Sabaawy HE, Hart RP, Schachner M. MicroRNA miR-133b is essential for functional recovery after spinal cord injury in adult zebrafish. Eur J Neurosci. 2011; 33(9):1587–1597. [PubMed: 21447094]

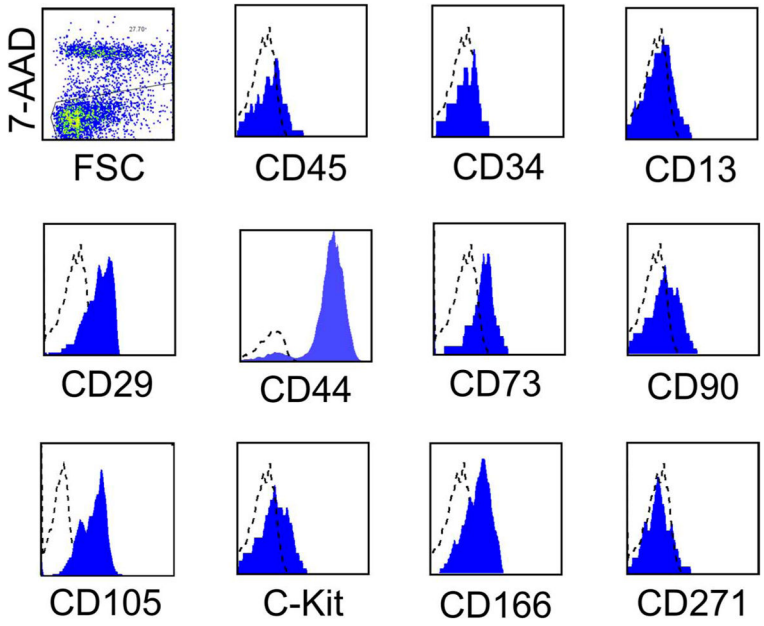

Figure 1.

The phenotype of primary canine ABMCs. Histograms of adherent bone marrow cells (ABMCs) from canine bone marrow (BM) samples that were isolated and cultured for 72 h on poly-L-lysine, lifted with accutase, and stained in a representative study for the specified cell surface markers. Dead cells were excluded using 7-aminoactinomycin D (7-AAD). A representative analysis is shown. FSC, forward scatter; CD45, cluster of differentiation 45.

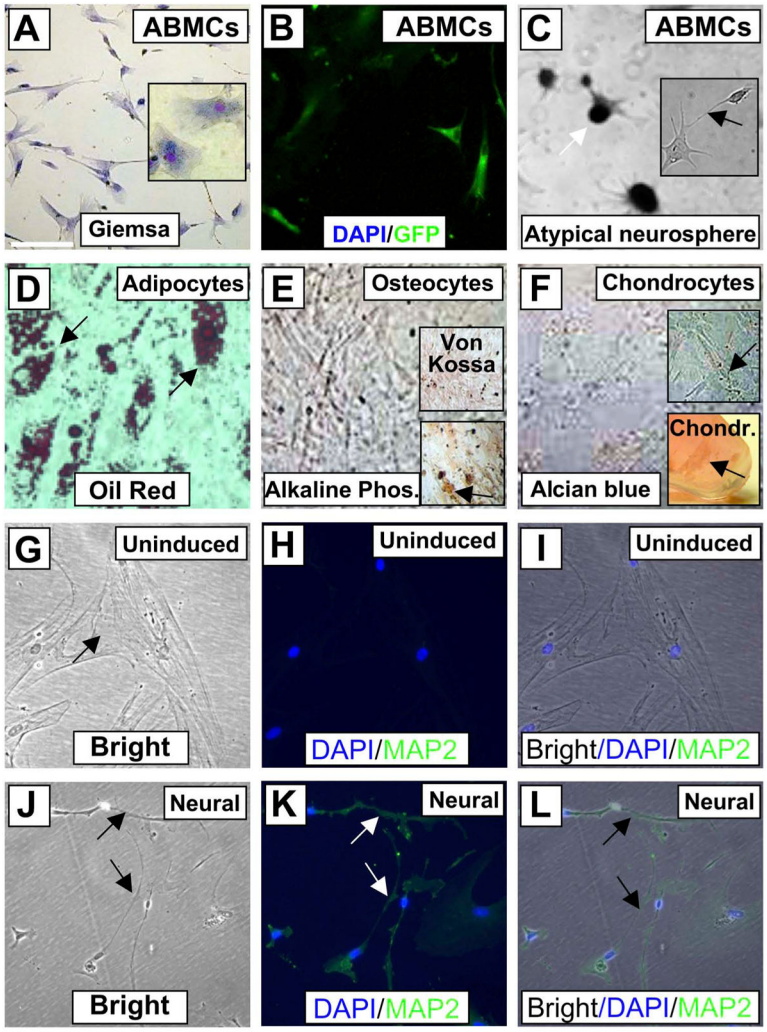

Figure 2.

Canine ABMC tripotency and neural induction. (A) Canine adherent BM cells isolated after 72 h (ABMCs) and stained with Giemsa. Inset shows a higher-power image of the cells. (B) Canine ABMCs transfected with GFP with ~95% efficiency. All cells in this field are positive for green fluorescent protein (GFP). (C) Neural induction of ABMCs after 1 week showing atypical neurospheres (white arrow) and extended dendrites (arrow in inset). (D) ABMCs induced for adipocytes and stained with oil red. (E) Osteocyte differentiation with Von Kossa staining (upper inset) and alkaline phosphatase staining (lower inset). (F) Alcian blue staining of ABMCs induced for chondrocytes in either tissue culture plate (upper inset) or as chondroitin sulfate aggregates (arrow) in a tube 3D culture (lower insert). (G–L) Bright and GFP images of uninduced control ABMCs (G–I) and ABMCs induced for neural differentiation and stained for the neuronal dendrite-specific marker microtubule-associated protein 2 (MAP2). Notice that uninduced cells are negative for MAP2 (H). After 12 days, induced cells demonstrate extended dendrites connecting neural-like cells that are positive for MAP2 (J–L). Nuclei were counterstained using 4′,6-diamidino-2-phenylindole (DAPI). Scale bars: 20 μm (A–L).

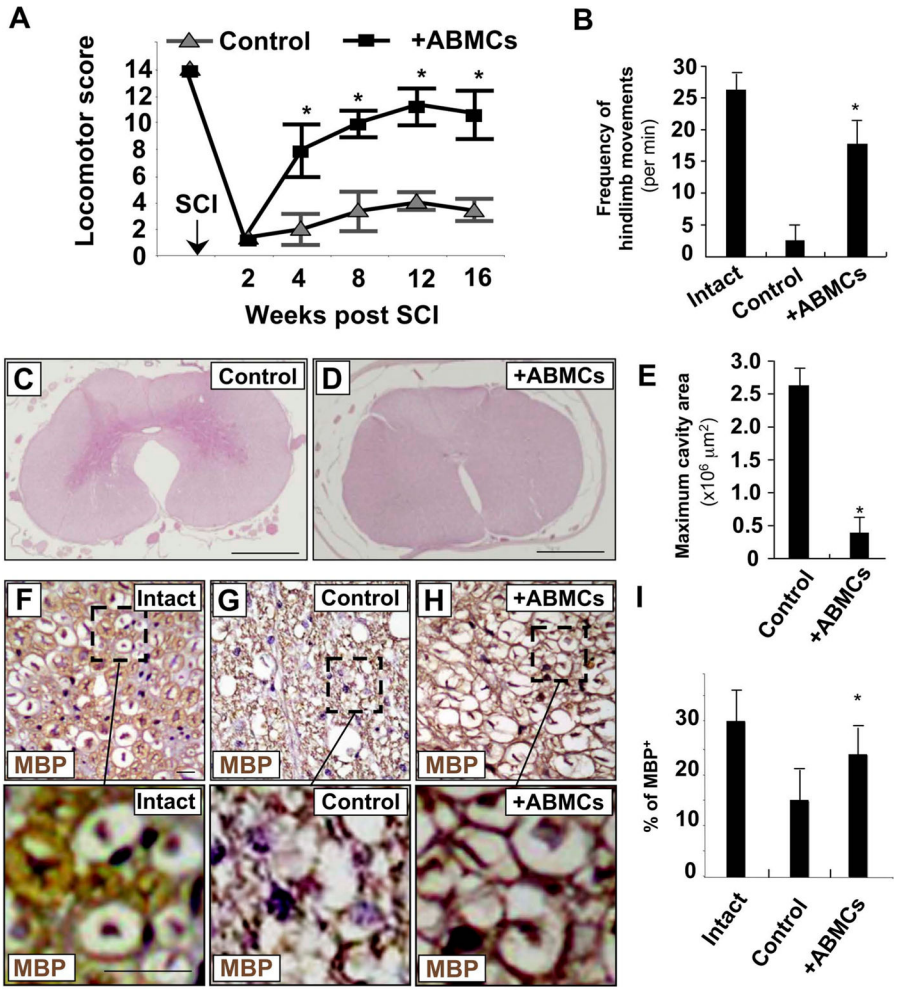

Figure 3.

Histopathological findings at 16 weeks post-ABMC therapy in the canine SCI model. (A) Locomotor scores of dogs at baseline and 2, 4, 8, 12, and 16 weeks after SCI. ABMCs were used for delayed transplantation in the second week after SCI. (B) Increase in hindlimb movements in dogs treated with autologous ABMCs compared to controls. (C) The epicenter of injured canine spinal cord in the control group stained with hematoxylin and eosin (H&E) and showing marked vacuolation and glial scarring. (D) The epicenter of the injured spinal cord of a dog from group B treated with autologous ABMCs, revealing histological signs of injury repair with less cavitation. (E) Quantitative analysis of cavity areas showing significant decrease in cavities in dogs treated with autologous ABMCs. (F–H) Myelin basic protein (MBP) immunostaining of intact spinal cord in intact dog (F), control SCI dog (G), and SCI dog treated with autologous ABMCs from group B (H). (I) Recovery of myelin basic protein to near normal levels with autologous ABMCs. Scale bars: 20 µm (C–D and F–H).

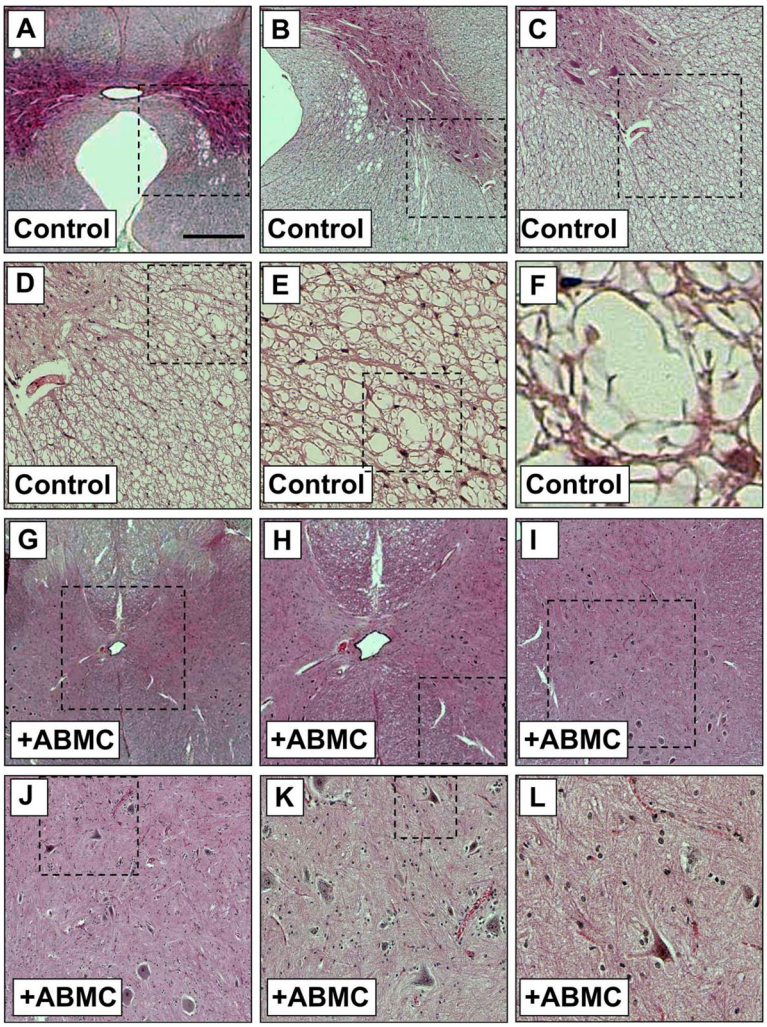

Figure 4.

Histological findings at 16 weeks post-ABMC therapy in the canine SCI model. (A–F) The epicenter of injured canine spinal cord in the control group stained with H&E and showing marked vacuolation and glial scarring. (G–L) The epicenter of injured spinal cord of a dog from group B treated with autologous ABMCs, revealing histological signs of injury repair with less cavitation. Images are sequential with higher magnification of the outlined areas in the following panel. Scale bars: 800 μm (A and G), 200 μm (B and H), 100 μm (C and I), 50 μm (D and J), 25 μm (E and K), and 6 μm (F and L).

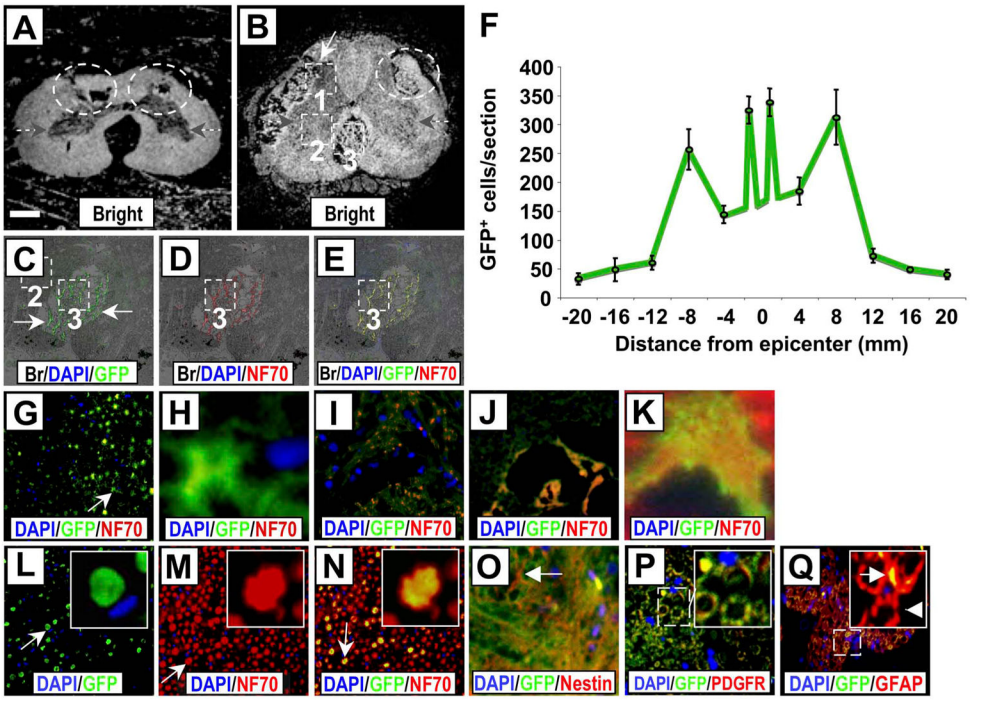

Figure 5.

Multicolor immunofluorescence staining of SCI sections from dogs treated with autologous ABMCs. (A, B) Cross section of SCI from control dog (A) showing cavitation (circled areas) and from a ABMC-treated dog from group B (B) showing less cavitation within the gray matter (gray arrows) (area 1), white matter (areas 2, 3), and well-organized tissue bridging the spinal cord gap (area 3) (white arrow) that was only observed in sections from dogs treated with autologous ABMCs. (C–E) Sections are higher-power overlay of bright images and fluorescent images of nuclear marker DAPI (blue), GFP (green) as a marker for transplanted ABMCs, and neurofilament 70 (NF70; red) as a neuronal maker within area 3. GFP expression was widespread in both the gray and white matter and the surrounding nerve roots. (F) Distribution of GFP^+ cells according to distance from epicenter. (G) Area 2 in the white matter of spinal cord showing GFP staining. (H) Higher-power image of a GFP^+ cell in G (arrow). (I) Area 1 in the gray matter of spinal cord showing colocalized GFP and NF70 staining. (J) Higher magnification of white matter area 2 of the injured cord showing colocalized GFP and NF70 staining. (K) Higher-power image of a GFP^+ and $NF70^+$ axon from J. (L–N) Area 3 of cross section in ventral funiculus potentially containing anterior corticospinal tracts. Insets showing higher magnification of an axon (arrow) with GFP colocalized with NF70. (O) Colocalized GFP and nestin staining in cells with neural morphology (arrow). (P) Colocalized GFP and platelet-derived growth factor receptor (PDGFR) staining; inset shows magnification of the outlined area. (Q) Colocalized GFP and glial fibrillary acidic protein (GFAP) staining, inset shows magnification of the outlined area. Arrow in inset indicates GFP^+ axon, while arrowhead points to an axon lacking GFP expression. DAPI is used for nuclear staining in all sections. Scale bars: 800 μm (A and B), 200 μm (C–E), 50 μm (G and J, L–Q), 20 μm (I), and 5 μm (H, K), and inserts (L–N and P–Q).

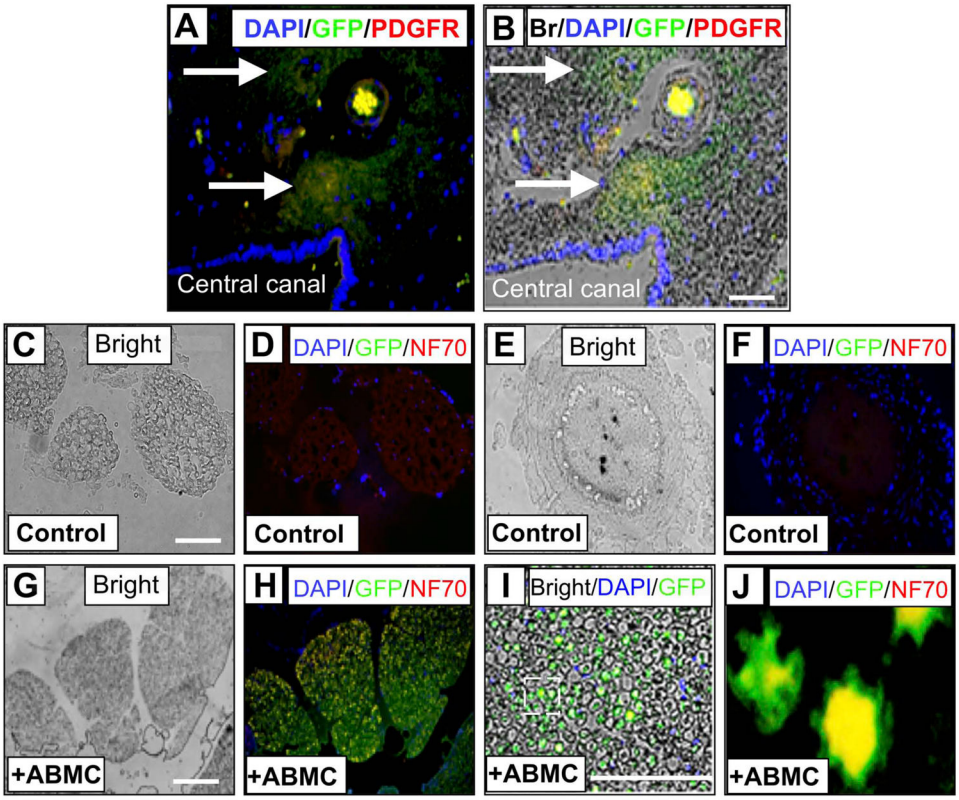

Figure 6.

Immunofluorescence staining of ABMC-derived cells positive for GFP and PDGFR at central canal and white matter spinal cord sections. (A) Fluorescent images of nuclear marker DAPI (blue), GFP (green) as a marker for transplanted canine ABMCs, and PDGFR (red) marker of neural progenitor cells near the central canal and associated with small vessels within the spinal cord. DAPI-positive nuclei lining the central canal are seen at the lower left area. (B) Overlay of the fluorescent images on the bright field showing GFP-positive cells coexpressing PDGFR within the spinal cord gray matter surrounding the central canal. (C–F) Spinal cord section from a control dog. (G–J) Section of spinal cord from dog treated with autologous ABMCs. (C) Bright field section and (D) fluorescent images of nuclear marker DAPI (blue), GFP (green), and NF70 (red) neuronal marker. (E) and (F) Higher magnification images from spinal cord sections of a control dog. No GFP expression was detected, while mild NF70 expression is seen in control sections. (G) Bright field and (H) fluorescent images of white matter in (E) stained with DAPI, GFP, and NF70. (I) Higher-power image of overlay of fluorescent images in (H) on the bright field in (G). (J) Higher magnification of outlined area in (I) showing GFP^{+} axons with colo-calized NF70 expression (yellow). Scale bars: 50 μm (A–B) and 100 μm (C–J).

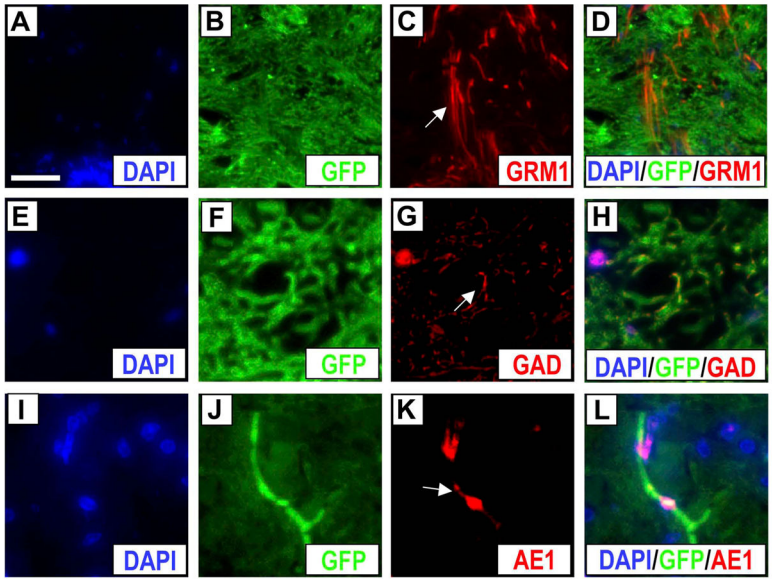

Figure 7.

Immunofluorescence staining of cell fate markers from dogs treated with autologous ABMCs. (A–L) Cross section of SCI from ABMC-treated dog (from group B) showing fluorescent images of nuclear marker DAPI (blue), GFP (green) as a marker for transplanted ABMCs, and either metabotropic glutamate receptor 1 (GRM1; excitatory glutamate) (A–D) (arrow in C shows GRM1 in red), glutamic acid decarboxylase [GAD, γ-aminobutyric acid (GABA)ergic inhibitory] (E–H) (arrow in G shows GAD in red), or AE1 (acetylcholinestrase-1) (I–L) (arrow in K shows AE1 in red), with left panels showing overlays. Scale bars: 20 μm (A–L).

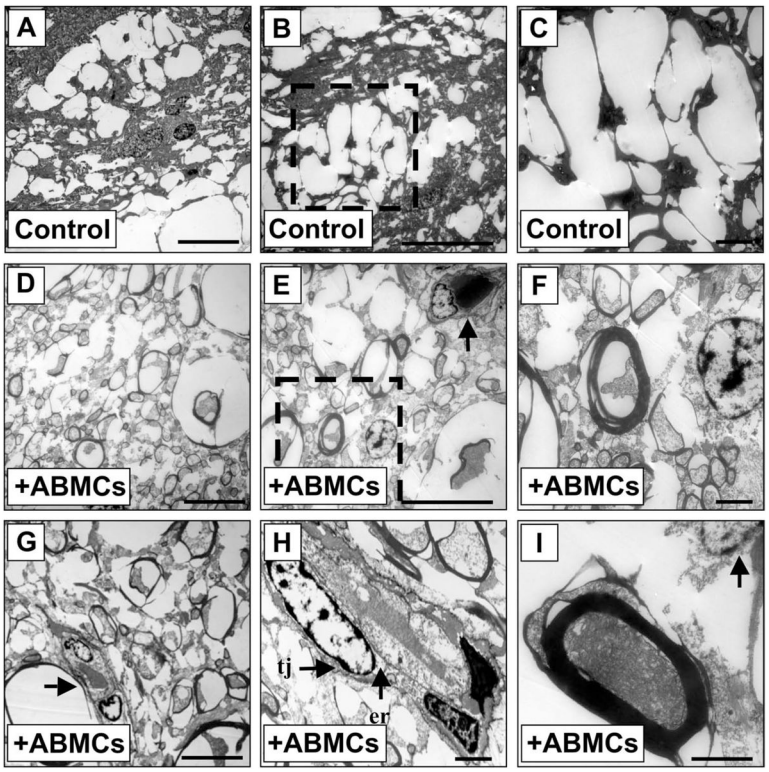

Figure 8.

Electron microscopic imaging of SCI sections after ABMC therapy. (A–C) Sections of SCI in control dogs demonstrating marked vacuolation and minimal axonal sparing that reconstituted less than 1% of sections. (A) Marked vacuolation in low-power field of SCI control dog. (B) Excessive vacuolation and scarring surrounding myelin-forming cell with no evidence for remyelination. (C) High-power image of area in (B). (D–I) Sections from SCI dogs treated with ABMCs demonstrating extensive remyelination and/ or axonal regeneration. (D) The regenerated axons were smaller in diameter. (E) Multiple axons were associated with multinucleated myelin-forming cells (arrow) suggesting lateral myelination. (F) Remyelinated axons with thick rim. (G) Myelin-forming cell (arrow) with multilobular nuclei engaging multiple axons. (H) Large myelin-forming oligodendrocyte with multiple nuclei and a surrounding basement membrane, dense cytoplasm, tight junction (tj) between the cell body and an oligodendrocyte process from another cell, and granular endoplasmic reticulum (er) in the perikaryon. (I) Remyelinated axon with thick rim engaging remyelinating cell on the top (arrow). Scale bars: 5 μm (A, B, D, E, and G) and 1 μm (C, F, H, and I).

Table 1

Recovery of Locomotor Activity After Intrathecal ABMC Injection in the Canine SCI Model

	Open Field Score (Mean ± SD)				
	Week 1	**Week 4**	**Week 8**	**Week 12**	**Week 16**
Control	1.9 ± 0.1	2.2 ± 1.2	3.6 ± 1.6	4.2 ± 0.6	3.8 ± 0.8
ABMCs	1.7 ± 0.2	8.0 ± 2.5	11 ± 0.9	11 ± 1.4	12 ± 1.2
ABMCs + (24 h)	1.8 ± 0.3	8.2 ± 2.1	10.9 ± 0.8	12 ± 1.2	11.6 ± 1.9
ABMCs + (72 h)	1.9 ± 0.1	7.7 ± 1.8	9.9 ± 1.2	12 ± 1.0	11 ± 1.8

ABMCs, adherent bone marrow cells; SCI, spinal cord injury.